EFFECT OF HEAT TREATMENT ON THE MICROSTRUCTURE AND HARDNESS OF A CAST INTERMETALLIC Ti-46Al-2W-0.5Si ALLOY

JURAJ LAPIN[1]*, ALENA KLIMOVÁ[1]

The effect of heat treatment on the microstructure and hardness of a cast intermetallic Ti-46Al-2W-0.5Si (at.%) alloy was studied. During annealing in the temperature range from 1350 to 1440 °C formation of grains with regular lamellar structure started in the vicinity of the surface and continued towards the central part of the annealing samples. The evolution of the grain size with the annealing time was found to follow a power law with time exponent n ranging from 0.35 to 0.38 and the activation energy for grain growth was determined to be 145 ± 11 kJ·mol^{-1} in the region of fully or nearly lamellar grains. Lower time exponent of 0.17 was measured in the region of originally equiaxed grains with duplex type of microstructure during annealing at 1415 and 1440 °C up to 5 h. The annealing temperature, time and cooling rate affected Vickers microhardness and hardness. The negligible difference in Vickers hardness values between different regions of the annealed samples was achieved after annealing at 1440 °C for 5 h.

K e y w o r d s: intermetallics, titanium aluminides, TiAl, heat treatment, microstructure, mechanical properties

VPLYV TEPELNÉHO SPRACOVANIA NA MIKROŠTRUKTÚRU A TVRDOSŤ ODLIEVANEJ INTERMETALICKEJ ZLIATINY Ti-46Al-2W-0,5Si

Študovali sme vplyv tepelného spracovania na mikroštruktúru a tvrdosť odlievanej intermetalickej zliatiny Ti-46Al-2W-0,5Si (at.%). V priebehu žíhania v teplotnom intervale od 1350 do 1440 °C začali smerom od povrchu do stredu žíhaných vzoriek rásť zrná s pravidelnou lamelárnou štruktúrou. V oblasti s lamelárnou alebo takmer lamelárnou štruktúrou pred žíhaním sme zistili mocninovú závislosť veľkosti zrna od času žíhania s časovým exponentom n v rozsahu od 0,35 do 0,38 a vypočítali sme aktivačnú energiu pre rast zrna 145 ± 11 kJ·mol^{-1}. Nižší časový exponent 0,17 sme určili pri teplotách žíhania 1415 a 1440 °C a pri čase do 5 h v oblastiach s duplexnou mikroštruktúrou pred žíhaním. Teplota žíhania, čas žíhania a rýchlosť ochladzovania výrazne ovplyvnili mikrotvrdosť a

[1] Institute of Materials and Machine Mechanics, Slovak Academy of Sciences, Račianska 75, 831 02 Bratislava, Slovak Republic

* corresponding author, e-mail: ummslapi@savba.sk

tvrdosť. Zanedbateľné rozdiely medzi hodnotami tvrdosti rôznych oblastí žíhaných vzoriek sme zistili po 5 h žíhania pri teplote 1440 °C.

1. Introduction

In recent years ordered TiAl based intermetallic alloys have been extensively studied as potential high-temperature materials in the gas turbine industry. The low density, high stiffness, good oxidation resistance and interesting mechanical properties have made TiAl based alloys attractive candidates for use in low-pressure stage of gas turbine engines or for turbocharger of diesel engines [1–5].

Of the numerous microstructures that can be developed in TiAl based alloys, the fully lamellar or nearly lamellar microstructure consisting of TiAl (γ-phase) and Ti_3Al (α_2-phase) exhibits better creep properties than duplex material [6, 7]. Formation of lamellar structure results from the precipitation of γ-lamellae in either a disordered α (Ti-based solid solution with hexagonal crystal structure) or an ordered α_2-matrix [8]. However, due to segregation of alloying elements, large cast components such as turbine blades may exhibit various microstructures ranging from fully or nearly lamellar in the vicinity of blade surface to duplex ones in the central part [7]. Such microstructural changes result in large local variations of mechanical properties of investment cast polycrystalline blades. Therefore, it is of great interest to investigate heat treatment conditions for processing cast components with homogeneous microstructure and optimised mechanical properties.

The aim of the present paper is to study the effect of heat treatment on the structure and hardness of an investment cast Ti-46Al-2W-0.5Si (at.%) alloy. As was shown recently [9, 10], nearly fully lamellar structure composed of regular γ- and α_2-phases can be achieved in this alloy by directional solidification techniques. The alloy was developed by Nazmy and Staubli [11] for investment cast turbine blades with improved creep properties. In creep resistant alloys, tungsten is known to act most effectively as solid solution strengthener and stabiliser of β-phase (Ti-based solid solution with cubic crystal structure). However, tungsten can segregate in dendrite cores, producing a detrimental effect on creep resistance. The addition of silicon to γ-TiAl alloy improves high-temperature oxidation resistance. The coherent Ti_5Si_3 particles formed through eutectoid transformation along lamellar interfaces enhance creep resistance and inhibit dynamic recrystallisation [5, 12].

2. Experimental procedure

Alloy with the chemical composition given in Table 1 was provided by Alstom Ltd in the form of a part of investment cast turbine blade [7]. The samples for heat treatment with dimensions of $7 \times 7 \times 10$ mm were cut from selected regions of the turbine blade by electro-spark machining, as illustrated in Fig. 1. The selected positions in the turbine blade assured reproducible microstructure in all samples

Table 1. Chemical composition (at.%)

Ti	Al	W	Si	O	N	Fe
Bal.	45.64	2.00	0.48	0.15	0.03	0.04

before annealing. The surface of each annealing sample contained two opposite planes with original surface of the turbine blade and four other surface planes were formed by electro-spark machining.

The samples were solution annealed at temperatures of 1350, 1380, 1415, and 1440 ℃ for various times ranging from 1 to 12 h in a resistance furnace under dynamic argon atmosphere (argon purity of 99.995 %). After annealing the samples were cooled to room temperature at a cooling rate of $10\,℃\cdot s^{-1}$. In the case of the samples annealed at 1440 ℃, two additional cooling rates of 2 and $60\,℃\cdot s^{-1}$ were applied. All annealed samples were cut in a direction perpendicular to the blade surface, so that the original blade surfaces remained visible on the transverse section of metallographic samples.

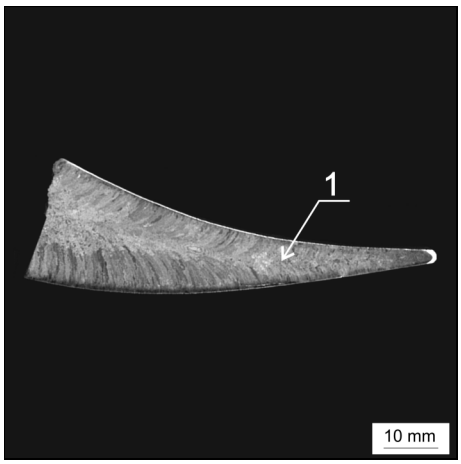

Fig. 1. Macrostructure on a transverse section of the part of turbine blade with marked position of annealing sample.

The Vickers microhardness and hardness measurements of studied samples were performed at the loads of 0.42 and 294.2 N, respectively. The loading time was 10 s.

The microstructure evaluation was performed by optical microscopy (OM), scanning electron microscopy (SEM) and energy-dispersive spectrometry (EDS). OM and SEM samples were prepared using standard metallographic techniques and etched in a reagent of 100 ml H_2O, 6 ml HNO_3 and 3 ml HF. Quantitative metallographic analysis was performed on digitalised micrographs using a computerised image analyser.

3. Results

3.1 Microstructure of the as-received material

Fig. 2a shows an example of typical microstructure of the samples before annealing. In the region I, the structure was composed of a surface layer with a

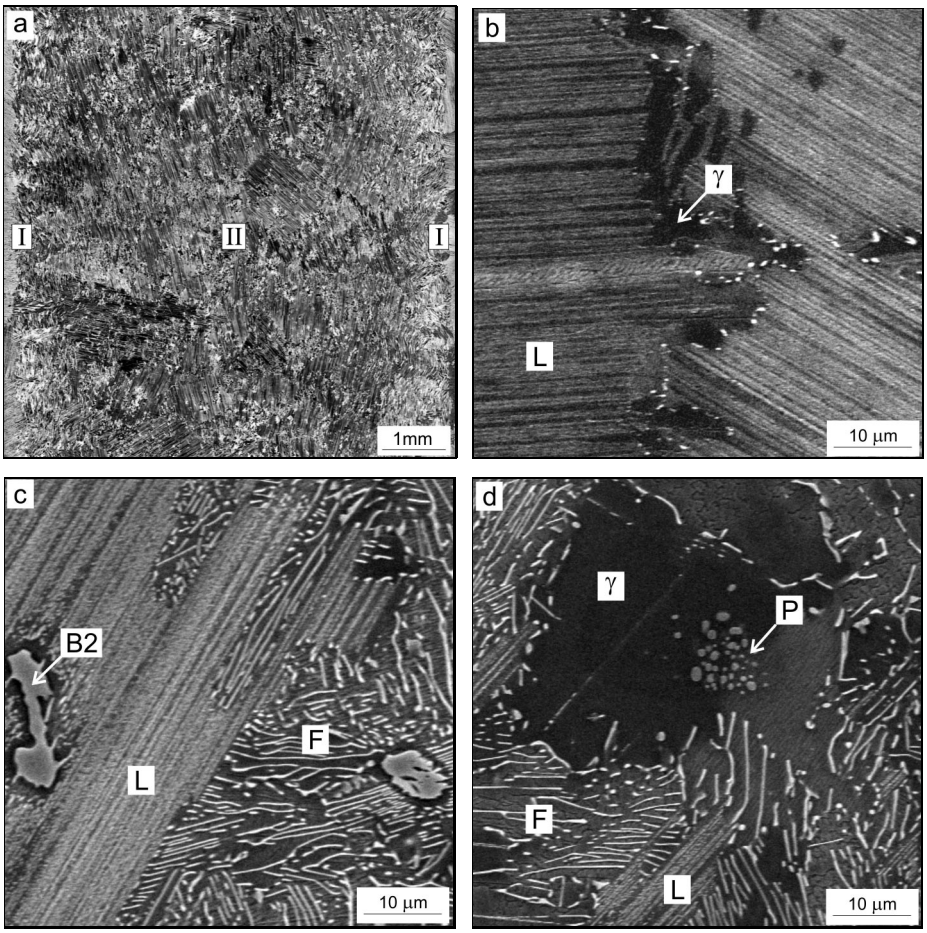

Fig. 2. Micrographs showing typical microstructure of the samples before annealing: (a) typical microstructure of annealing samples, OM; (b) regular lamellar microstructure and γ-phase region formed within columnar grain structure, SEM; (c) regular lamellar microstructure, irregular lamellar microstructure and B2-particles in the central part of annealing samples with equiaxed grain structure, SEM; (d) Ti_5Si_3 precipitates within the γ-phase region in the central part of samples, SEM. L – regular lamellar microstructure, F – irregular lamellar microstructure, P – Ti_5Si_3 precipitates.

thickness of about 200 μm containing equiaxed grains and layer of columnar grains with a thickness of about 1000 μm. Region II contained equiaxed grains formed in the central part of the sample. The equiaxed grains in the vicinity of the blade surface were fully lamellar composed of α_2-phase (Ti_3Al phase with DO_{19} crystal structure) and γ-phase (TiAl phase with $L1_0$ crystal structure). The columnar grains with a diameter of about 300 μm were nearly lamellar consisting of fully

lamellar regions and γ-phase (dark colour phase) with fine B2-precipitates (bright colour phase) formed at the columnar grains boundaries, as seen in Fig. 2b. The equiaxed grains in the central part of the turbine blade were composed of regular lamellar regions (L) with coarse B2 precipitates (Fig. 2c), γ-regions and irregular lamellar regions (F) consisting of the α_2, γ and B2 phases. In some cases, the γ--regions contained coarse Ti_5Si_3 precipitates, as illustrated in Fig. 2d. In addition,

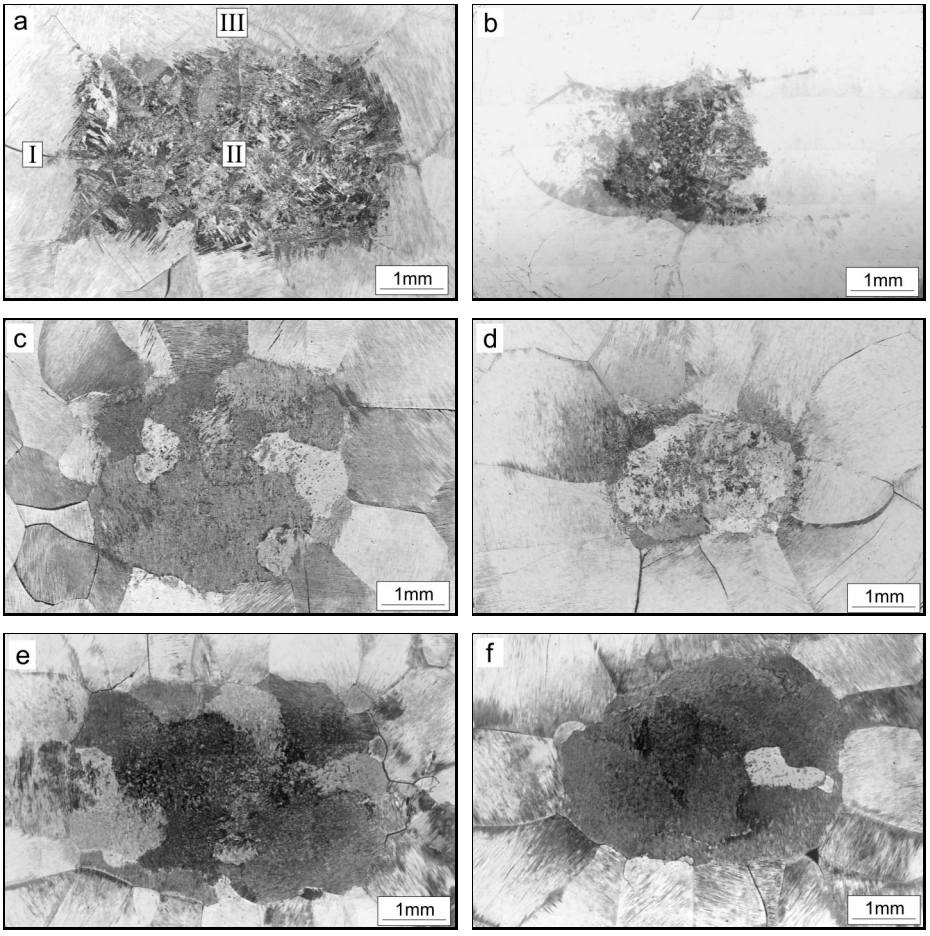

Fig. 3. Optical macrographs showing the effect of annealing temperature and time on the microstructure of the annealed samples cooled from the annealing temperatures at the cooling rate of $10\,℃\cdot s^{-1}$: (a) 1380 ℃/5 h; (b) 1380 ℃/8 h; (c) 1415 ℃/5 h; (d) 1415 ℃/8 h; (e) 1440 ℃/5 h; (f) 1440 ℃/8 h. I – region of fully lamellar grains formed in the vicinity of the original blade surface, II – region of duplex structure, III – region of fully lamellar grains formed in the vicinity of the surface affected by spark machining.

the studied as-received material contained fine Ti_5Si_3 and B2 precipitates formed at lamellar γ/α_2 interfaces [7].

3.2 Effect of the annealing temperature and time on the microstructure

Metallography analysis revealed that formation of lamellar structure was not homogeneous in the whole volume of the samples during the heat treatment. The formation of fully lamellar structure started within new recrystallised grains in the vicinity of original blade surface (region I) and the surface affected by spark machining (region III) and continued towards the central part of the sample (region II), as illustrated in Fig. 3a. Figs. 3a to 3f show the effect of the annealing temperature and time on the microstructure of the heat-treated samples. Fig. 4 summarises the evolution of the volume fraction of regular lamellar, γ-phase and

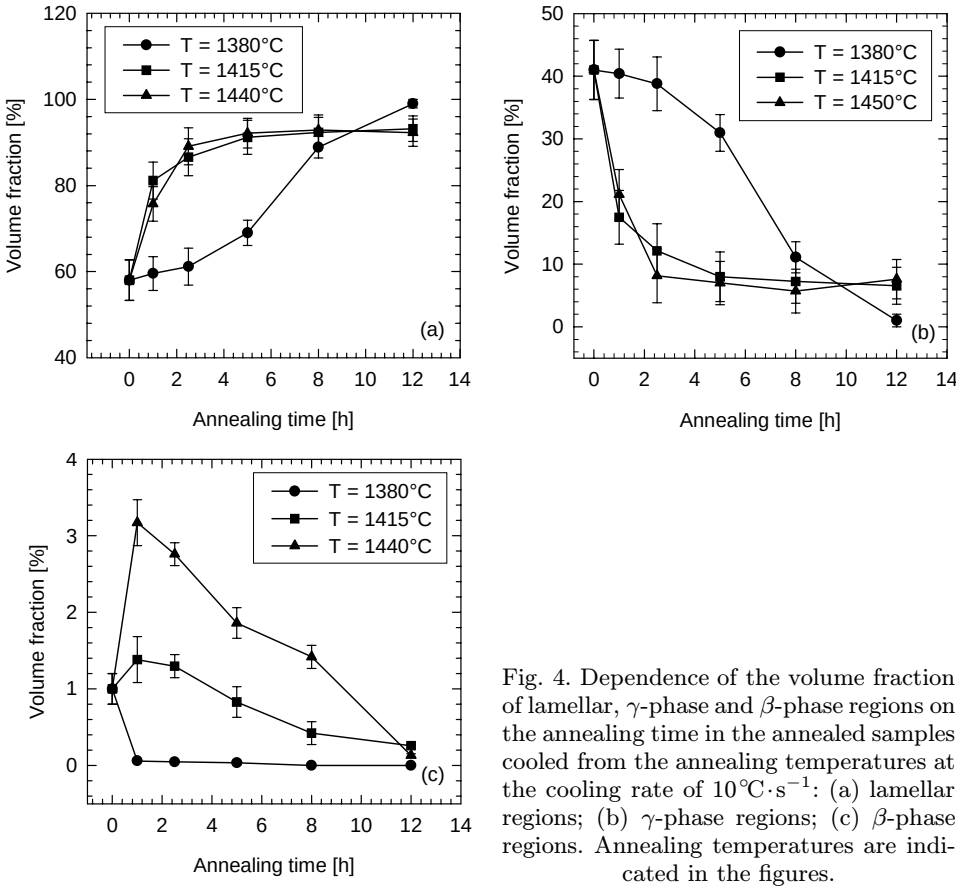

Fig. 4. Dependence of the volume fraction of lamellar, γ-phase and β-phase regions on the annealing time in the annealed samples cooled from the annealing temperatures at the cooling rate of $10\,^{\circ}\mathrm{C}\cdot\mathrm{s}^{-1}$: (a) lamellar regions; (b) γ-phase regions; (c) β-phase regions. Annealing temperatures are indicated in the figures.

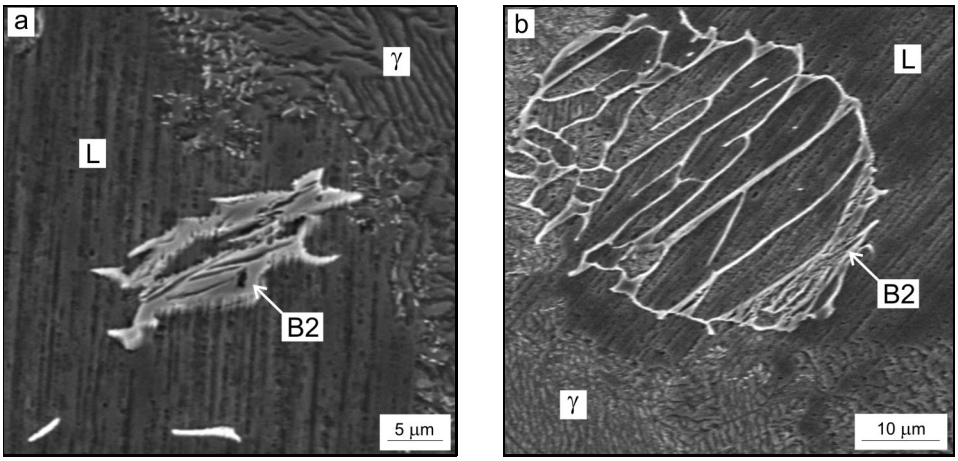

Fig. 5. SEM micrographs showing the morphology of B2-particles: (a) 1415 °C/1 h; (b) 1440 °C/1 h. L – regular lamellar region.

β-phase regions with the annealing time for the samples cooled from the annealing temperatures at the cooling rate of 10 °C·s^{-1}. Annealing at 1415 and 1440 °C up to 8 h significantly increases volume fraction of regular lamellar regions (Fig. 4a) and decreases volume fraction of the γ-phase regions (Fig. 4b) in comparison with those at 1380 °C. However, such high annealing temperatures cause the formation of high temperature β-phase in the microstructure (Fig. 4c). Nearly fully lamellar structure can be achieved after annealing at 1380 °C for 12 h (Fig. 4a). Fig. 5 shows different morphology of the high temperature β-phase. As seen in this figure, lower annealing temperature of 1415 °C caused the formation of coarse β-phase particles (Fig. 5a). At higher annealing temperature of 1440 °C, the high temperature β--phase forms a network within the annealed samples (Fig. 5b). During annealing at 1380 °C high temperature β-phase formation was not observed.

3.3 Effect of the cooling rate on the microstructure

Fig. 6 illustrates the effect of the cooling rate on the microstructure of the samples which were solution annealed at 1440 °C for 5 h. Cooling at the lowest cooling rate of 2 °C·s^{-1} resulted in formation of well-developed lamellar microstructure within recrystallised grains in the regions I and III (Fig. 6a). Higher cooling rates of 10 and 60 °C·s^{-1} resulted in finer lamellar structure, as illustrated in Figs. 6b and 6c. It should be noted that the fine lamellar structure could not be clearly distinguished on the optical micrograph shown in Fig. 6c, which appears as a single-phase region. Fig. 7 shows the dependence of the volume fractions of co-existing phases in the whole volume of the annealed samples on the cooling rate.

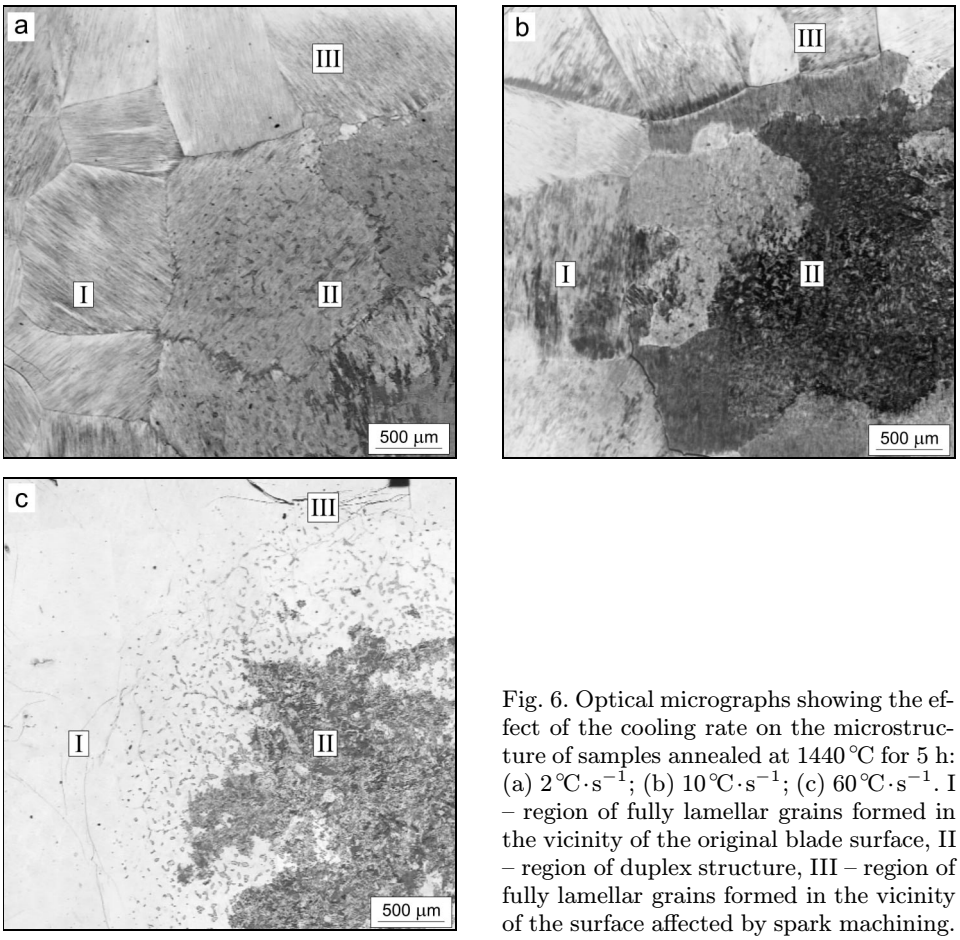

Fig. 6. Optical micrographs showing the effect of the cooling rate on the microstructure of samples annealed at 1440 °C for 5 h: (a) 2 °C·s^{-1}; (b) 10 °C·s^{-1}; (c) 60 °C·s^{-1}. I – region of fully lamellar grains formed in the vicinity of the original blade surface, II – region of duplex structure, III – region of fully lamellar grains formed in the vicinity of the surface affected by spark machining.

Increasing cooling rate decreases volume fraction of the lamellar regions, increases volume fraction of the γ-phase regions and has no effect on the volume fraction of the high-temperature β-phase.

3.4 Grain growth

During the solution annealing the grain growth kinetics in the vicinity of the original blade surface (region I) was different from that in the central part (region II) and in the vicinity of surfaces affected by electro-spark machining (region III), as shown in Fig. 3. Therefore, the grain size was measured separately in the region I with lamellar or nearly lamellar microstructure and regions II and III with duplex type of microstructure before heat treatment.

In the region I, the measured grain size d increased with the increase of the

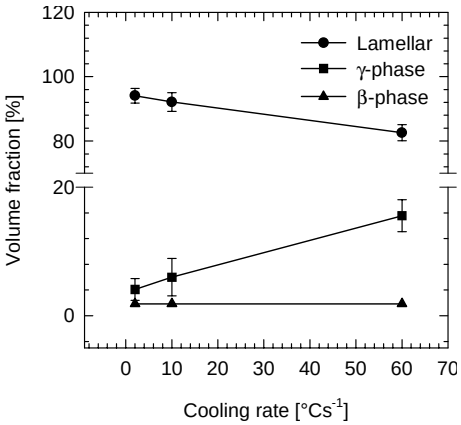

Fig. 7. Dependence of the volume fraction of regular lamellar regions, γ-phase and β-phase on the cooling rate after annealing at 1440 ℃ for 5 h.

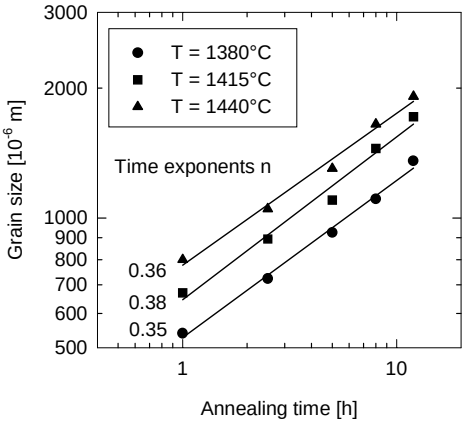

Fig. 8. Variations of the grain size with the annealing time in the region I. The annealing temperatures and measured time exponents are indicated in the figure.

annealing time according to a power law

$$d = kt^n, \tag{1}$$

where k is a material constant at a given temperature, t is the annealing time and n is the time exponent. Fig. 8 shows the dependence of the grain size on the annealing time in the region I. The time exponent determined by linear regression analysis was found to vary between 0.35 and 0.38. The regression coefficients of these fits are better than $r^2 = 0.97$. These measured time exponents are comparable with those of $n = 0.4$ determined by Zhang et al. [4] for Ti-48Al-2W-0.5Si (at.%) alloy but lower than theoretically expected value of 0.5 corresponding to parabolic grain growth of pure metals.

If the size of recrystallised grains in the region I at $t = 0$ is negligible in comparison with that at longer annealing time, the kinetic equation for the grain growth can be written in the form [4]

$$d = k_0 t^n \exp\left(-\frac{Q}{RT}\right), \tag{2}$$

where k_0 is a material constant, Q is the activation energy for grain growth, R is the universal gas constant, and T is the absolute temperature. Fig. 9 shows the dependence of the grain size on the annealing temperature in the form of an

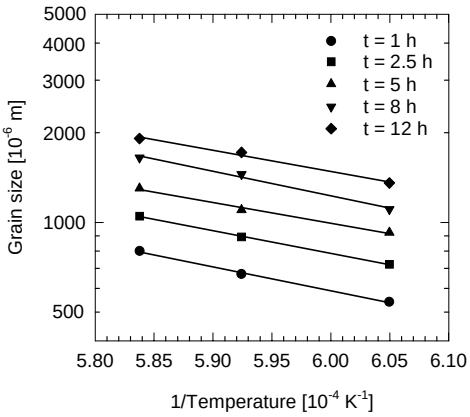

Fig. 9. Arrhenius type of diagram showing the dependence of the grain size on the temperature. The annealing times are indicated in the figure.

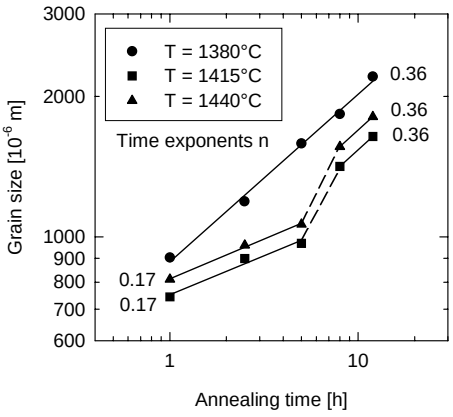

Fig. 10. Variations of the grain size with the annealing time in the regions II and III. The annealing temperatures are indicated in the figure.

Arrhenius diagram. Using linear regression, the activation energy for the grain growth calculated for five annealing times at three annealing temperatures was determined to be 145 ± 11 kJ·mol^{-1}.

Fig. 10 shows the variation of the grain size with the annealing temperature in the regions II and III. In spite of the fact that the samples contained statistically the same grain size before annealing, grain coarsening was more intensive at 1380 ℃ than at higher temperatures. The evolution of the grain size with annealing time at 1380 ℃ follows Eq. (1) with the time exponent $n = 0.36$. On the contrary, the evolution of the average grain size at 1415 and 1440 ℃ is not continuous and can be divided into three different stages. During the first stage up to the annealing time of 5 h, the grain growth follows the power law with a time exponent of 0.17, as shown in Fig. 10. The second stage of coarsening was observed during annealing from 5 to 8 h. This stage was connected with partial dissolution of coarse β-particles, which resulted in an intensive coarsening of homogenised grains in the region III and elimination of small ones. The third stage of coarsening characterised by a time exponent of 0.36 is similar to that at 1380 ℃. However, the average grain size at 1415 and 1440 ℃ was lower than that at 1380 ℃.

3.5 Vickers microhardness and hardness

Fig. 11 shows the effect of the annealing temperature on the Vickers microhardness in the samples annealed for 5 h and cooled to room temperature at the cooling rate of 10 ℃·s^{-1}. Increasing annealing temperature results in a decrease of

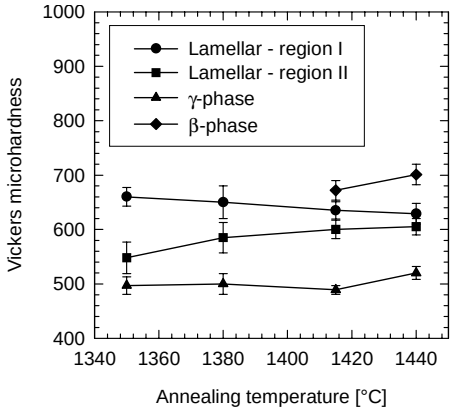

Fig. 11. Dependence of Vickers microhardness on the annealing temperature after annealing for 5 h and cooling at the rate of $10\,^{\circ}\mathrm{C}\cdot\mathrm{s}^{-1}$. Different regions are indicated in the figure.

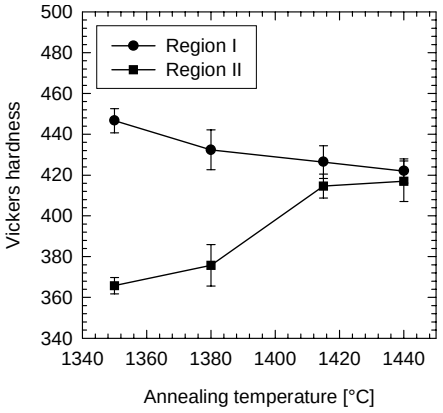

Fig. 12. Dependence of Vickers hardness on the annealing temperature after annealing for 5 h and cooling at the rate of $10\,^{\circ}\mathrm{C}\cdot\mathrm{s}^{-1}$. Different regions are indicated in the figure.

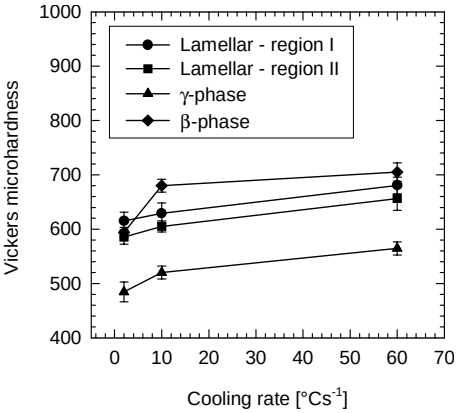

Fig. 13. Dependence of Vickers microhardness on the cooling rate after annealing at 1440 °C for 5 h. Different regions are indicated in the figure.

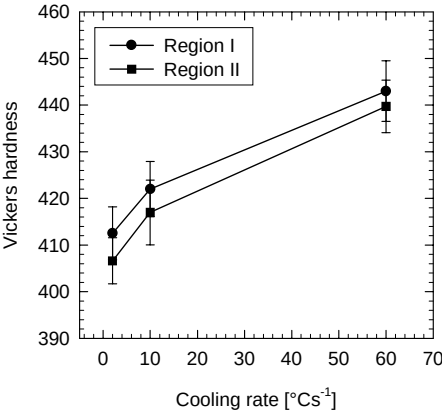

Fig. 14. Dependence of Vickers hardness on the cooling rate after annealing at 1440 °C for 5 h. Different regions are indicated in the figure.

the microhardness of the regular lamellar structure in the region I. On the contrary, the microhardness of regular lamellar structure in the region II increases as well as the microhardness of the regions containing high-temperature β-phase formed

at 1415 and 1440 ℃. The annealing temperature does not significantly affect the microhardness of the γ-regions. Fig. 12 shows the evolution of the hardness with the annealing temperature. As in the case of microhardness measurements, the hardness of regular lamellar structure in the region I decreases and the hardness of the multiphase region II increases with increasing annealing temperature.

Fig. 13 shows the effect of the cooling rate on the Vickers microhardness in the samples solution annealed at 1440 ℃ for 5 h. Increasing cooling rate from 2 to 60 ℃·s^{-1} increases the microhardness of regular lamellar structure in the regions I and II, γ-phase and regions containing high-temperature β-phase. Fig. 14 shows the evolution of Vickers hardness with the cooling rate. As in the case of the microhardness, the hardness increases with the increasing cooling rate in the regions I and II.

4. Discussion

4.1 Microstructure after heat treatment

As shown by Yin et al. [5], both higher content of W and lower content of Al favour formation of high-temperature β-phase. However, the effect of W on β--phase formation is more important than the effect of Al. The results of the present work suggest that local microstructural variations within the samples significantly affected the formation of the high-temperature β-phase during annealing at 1415 and 1440 ℃. Table 2 shows the average chemical composition in the regions I and II before heat treatment. While the content of Al is at the same level in both regions, the region II is enriched with W. This local enrichment resulted in an intensive formation of coarse β-particles in the region II but no particles were formed within recrystallised fully lamellar grains in the regions I and III. In spite of the fact that the formation of high-temperature β-phase in W modified γ-TiAl alloys has been reported in several articles [5, 6, 12, 13], due to a lack of research work on Ti--Al-W phase diagram, it is not easy to elucidate how small variations in chemical composition, which is the case of the studied alloy, exactly affect its formation and equilibrium with other coexisting phases. It should be noted that available Ti-Al-W phase diagrams of Kainuma et al. [14] or pseudobinary Ti-Al-W-Si phase diagram of Gil et al. [15] are defined only for temperatures up to 1300 ℃.

As was shown by Denquin and Naka [8], formation of lamellar structure results from the precipitation of γ-lamellae in either a disordered α- or an ordered

Table 2. EDS analysis of the average chemical composition (at.%) in different regions of the samples before annealing

Position	Ti	Al	W	Si
Region I	52.42 ± 1.28	45.98 ± 1.12	1.10 ± 0.22	0.50 ± 0.07
Region II	51.00 ± 1.65	46.01 ± 1.72	2.48 ± 0.82	0.49 ± 0.11

α_2-matrix. During continuous cooling from the α-phase field, the formation of γ--lamellae starts in the $\alpha + \gamma$ phase-field and is completed in the $\alpha_2 + \gamma$ phase-field. The whole sequence of the lamellar structure formation involves three stages: (1) change of the crystal structure from h.c.p. to f.c.c. by propagation of Shockley partial dislocations in the hexagonal matrix; (2) a chemical composition change through atom transfer by a combined shear and diffusion process, and (3) an ordering reaction of the f.c.c. structure leading to the final $L1_0$ γ-phase. The volume fraction of fully lamellar regions depends not only on the annealing temperature and time but also on the cooling rate, as shown in Fig. 7. Increase of the volume fraction of the γ-phase with increasing cooling rate resulted from massive transformation of the α-phase to the γ-phase predominantly in the region II. As shown by Xia et al. [16] in Ti-46Al-2Cr-2Nb and Ti-48Al-2Cr (at.%) alloys, regular lamellar structure was formed from the α-phase at low cooling rates. Higher cooling rates resulted in formation of Widmanstätten type structure or massive γ. Further increase of cooling rate led to a direct transformation of the α to the α_2-phase. The massive γ developed first at grain boundaries as lamellae in one of the grains and these lamellae intersected and spread into the adjacent grain in a massive manner without crystallographic orientation relationship to the grain being consumed [17]. Formation of massive γ is sensitive to chemical composition. As was shown by Hu and Botten [18], during rapid cooling low content of Al and high fraction of β stabilisers can result in formation of lath-like α instead of massive γ. The metallographic observations revealed that massive transformation occurred along some α-grain boundaries in the studied alloy, as shown in Fig. 15. It should be noted that formation of massive γ was more intensive at 1380 ℃ than at higher temperatures, as illustrated in Figs. 3 and 4b. This fact can be explained by the presence and stability of the high-temperature β-phase at 1415 and 1440 ℃, which reduce the tendency of the alloy to transform massively to γ-phase during cooling [18].

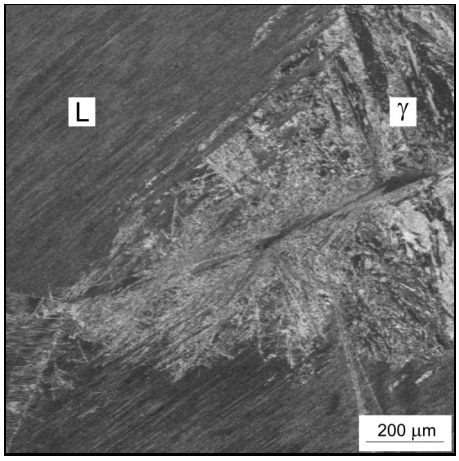

Fig. 15. SEM micrograph showing massive γ after annealing at 1380 ℃ for 5 h and subsequent cooling at 10 ℃·s^{-1}.

4.2 Grain growth

The activation energy for grain growth of 145 kJ·mol^{-1} in the region I is

comparable with that of 147 kJ·mol^{-1} determined by Zhang et al. [4] for the α--grain growth in Ti-48Al-2W-0.5Si (at.%) alloy. However, due to high annealing temperatures, it is not possible to compare this value with those for volume or grain boundary diffusion of Ti or Al in α- and γ-phase. As reported by Herzig et al. [19], temperatures higher than 1197 ℃ are too high for measuring reliably the grain boundary diffusion-related tails of penetration profiles and consequently to determine the activation energy for grain boundary diffusion. We can only refer to data measured in various Ti-Al systems for temperatures up to above 1000 ℃, where the activation energies for Ti grain boundary diffusion were determined to vary between 187 and 246 kJ·mol^{-1} in α-phase and between 112 and 118 kJ· ·mol^{-1} in γ-phase [19]. For bulk diffusion of Ti and Al the value of 250 and 360 kJ·mol^{-1} were determined for the temperatures up to 1197 ℃, respectively [19, 20]. Comparing the above mentioned values to the measured activation energy of 145 ± 11 kJ·mol^{-1} indicates that the grain growth in the region I can not be confirmed to be governed by the grain boundary or volume diffusion of Ti or Al in the α-phase.

Fig. 10 clearly shows anomalous grain growth in the region II and III. As was previously reported by Zhang et al. [4], lower time exponents of 0.2 during annealing of an intermetallic alloy with similar chemical composition resulted from a hindered α-grain growth by the γ-grains. However, such mechanisms were only effective up to the annealing time of about 0.3 h. In our case, the hindered grain growth is caused by formation of high-temperature β-particles in the microstructure at 1415 and 1440 ℃. The high temperature β-phase particles significantly retard the grain growth in the region II in comparison with that in the region I.

4.3 Effect of heat treatment on Vickers microhardness and hardness

Fig. 11 shows that the annealing temperature affects Vickers microhardness of lamellar regions and regions containing high-temperature β-phase after annealing for 5 h. As was shown in directionally solidified material [9], the microhardness of fully lamellar structure is affected by two basic parameters: interlamellar spacing and volume fraction of coexisting α_2- and γ-phases. Increasing volume fraction of harder α_2-phase and decreasing interlamellar spacing increase the microhardness. The mean values of interlamellar spacing determined by log-normal distribution function changed from 349 and 441 nm at 1350 ℃ to 373 and 405 nm at 1440 ℃ in the regions I and II, respectively. Hence, the difference between microhardness of lamellar microstructure in the regions I and II is caused by redistribution of alloying elements (see Table 2) resulting in small variations in the interlamellar spacing and solution and/or precipitation strengthening of coexisting phases. The increase of annealing temperature decreases chemical heterogeneity within the samples and consequently decreases differences between the microhardness values in the regions

I and II. The highest microhardness was measured in the regions containing high-temperature β-phase. Since these microhardness values were affected by the matrix (lamellar and/or massive γ), higher microhardness values after annealing at 1440 ℃ in comparison with that at 1415 ℃ were caused by a higher volume fraction and more effective strengthening effect of the β-phase in the form of a network than that in the form of coarse particles. Fig. 12 shows that higher annealing temperature during annealing for 5 h leads to more homogeneous hardness values in the whole volume of annealed samples. The negligible difference of Vickers hardness values between different regions was achieved after annealing at 1440 ℃ for 5 h.

The Vickers microhardness of lamellar region increases with increasing cooling rate (Fig. 13). This evolution can be explained by decreasing interlamellar spacing from 393 and 437 nm at the cooling rate of $2\,℃\cdot s^{-1}$ to 373 and 405 nm at the cooling rate of $10\,℃\cdot s^{-1}$ in the regions I and II, respectively. The interlamellar spacing at the highest cooling rate of $60\,℃\cdot s^{-1}$ could not be determined reliably by the means of SEM. The increase of the microhardness of the γ-phase and β-phase regions results from an increase of crystal defects such as dislocation density and number of vacancies in these regions [18]. The hardness increases with increasing cooling rate in both regions I and II. A negligible difference between hardness values in the regions indicates that chemical and consequently structural homogeneity was achieved after annealing at 1440 ℃ for 5 h.

It should be noted that microhardness measurements could be used for reliable prediction of the yield stress. In lamellar or nearly lamellar alloys, higher Vickers microhardness values HV_{m} indicate a higher room-temperature yield stress σ_{y} according to a linear relationship $\sigma_{\mathrm{y}} \propto HV_{\mathrm{m}}$ [9].

5. Conclusions

The effect of heat treatment on the structure and hardness of a cast intermetallic Ti-46Al-2W-0.5Si (at.%) alloy was studied. The following conclusions were reached:

1. Before annealing the structure of the annealed samples was composed of fully lamellar equiaxed grains, nearly lamellar columnar grains and equiaxed grains with duplex type of microstructure. The lamellar grains were composed of regular α_2- and γ-lamellae. The duplex type of microstructure contained regular lamellar regions, irregular lamellar regions, γ-rich regions and small volume fractions of fine and coarse B2- and Ti_5Si_3-precipitates.

2. During heat treatment formation of regular lamellar structure was not homogeneous in the whole volume of samples. Fully lamellar grains started growing in the vicinity of sample surface and continued towards the central part. Increasing annealing temperature and time increased volume fraction of regular lamellar regions and decreased volume fraction of the γ-regions. Nearly fully lamellar structure was achieved after annealing at 1380 ℃ for 12 h. Increasing cooling rate decreased the

volume fraction of the regular lamellar regions and increased the volume fraction of the γ-regions.

3. Annealing at 1415 and 1440 ℃ resulted in formation of high-temperature β-phase in the region of equiaxed grains with duplex type of microstructure before annealing. The volume fraction of the β-phase decreased with increasing annealing time.

4. The evolution of the grain size with the annealing time was found to follow a power law with time exponent n ranging from 0.35 to 0.38 and the activation energy for grain growth was determined to be 145 ± 11 kJ·mol^{-1} in the region of fully or nearly lamellar grains. Lower time exponent of 0.17 was measured in the region of originally equiaxed grains with duplex type of microstructure during annealing at 1415 and 1440 ℃ up to 5 h.

5. The annealing temperature, time and cooling rate affected Vickers microhardness and hardness. The negligible difference in the Vickers hardness values between different regions of the annealed samples was achieved after annealing at 1440 ℃ for 5 h.

Acknowledgements

The authors gratefully acknowledge the financial support of the Slovak Grant Agency for Science under the contract VEGA 2/1044/21 and the COST 522 project under the contract 51-98-9209-00/1999. They also express their thanks to Dr. M. Nazmy from ALSTOM Ltd for providing the experimental material.

REFERENCES

[1] DIMIDUK, D. M.: Mater. Sci. Eng. A, *A263,* 1999, p. 281.
[2] NAZMY, M.—STAUBLI, M.—ONOFRIO, G.—LUPINC, V.: Scripta Mater., *45,* 2001, p. 787.
[3] EVANGELISTA, E.—ZHANG, W. J.—FRANCESCONI, L.—NAZMY, M.: Scripta Metall. Mater., *33,* 1995, p. 467.
[4] ZHANG, W. J.—EVANGELISTA, E.—FRANCESCONI, L.: Mater. Sci. Eng. A, *A220,* 1996, p. 168.
[5] YIN, W. M.—LUPINC, V.—BATTEZZATI, L.: Mater. Sci. Eng. A., *A239–240,* 1997, p. 713.
[6] LUPINC, V.—YIN, W. M.—MALDINI, M.: In: Materials for Advanced Power Engineering 1998. Eds.: Lecomte-Beckers, J., Schubert, F., Ennis, P. J. Vol. 5, Part III, Forschungszentrum Jülich GmbH, Jülich 1998, p. 1239.
[7] LAPIN, J.—PELACHOVÁ, T.: In: 7th Liège Conference – Materials for Advanced Power Engineering 2002. Eds.: Lecomte-Beckers, J. Carton, M. Schubert, F. Ennis, P. J. Vol. 21, Part II, Forschungszentrum Jülich GmbH, Jülich 2002, p. 623.
[8] DENQUIN, A.—NAKA, S.: Acta Mater., *44,* 1996, p. 343.
[9] LAPIN, J.—ONDRÚŠ, Ľ.—NAZMY, M.: Intermetallics, *10,* 2002, p. 1019.
[10] LAPIN, J.—ONDRÚŠ, Ľ.: Kovove Mater., *40,* 2002, p. 161.
[11] NAZMY, M.—STAUBLI, M.: U.S.Pat.#5,207,982 and European Pat.#45505 BI.
[12] YU, R.—HE, L. L.—JIN, Z. X.—GUO, J. T.—YE, H. Q.—LUPINC, V.: Scripta Mater., *44,* 2001, p. 911.

[13] RECINA, V.—AHLSTRÖM, J.—KARLSSON, B.: Mater. Charact., *38,* 1997, p. 287.
[14] KAINUMA, R.—FUJITA, Y.—MITSUI, H.—OHNUMA, I.—ISHIDA, K.: Intermetallics, *8,* 2000, p. 855.
[15] GIL, I.—MUÑOZ-MORRIS, M. A.—MORRIS, D. G.: Intermetallics, *9,* 2001, p. 373.
[16] XIA, Q.—WANG, J. N.—YANG, J.—WANG, Y.: Intermetallics, *9,* 2001, p. 361.
[17] ZHANG, X. D.—GODFREY, S.—WEAVER, M.—STRANGWOOD, M.—THREADGILL, P.—KAUFMAN, M. J.—LORETTO, M. H.: Acta Mater., *44,* 1996, p. 3723.
[18] HU, D.—BOTTEN, R. R.: Intermetallics, *10,* 2002, p. 701.
[19] HERZIG, CH.—WILGER, T.—PRZEORSKI, T.—HISKER, F.—DIVINSKI, S.: Intermetallics, *9,* 2001, p. 431.
[20] HERZIG, CH.—PRZEORSKI, T.—MISHIN, Y.: Intermetallics, *7,* 1999, p. 389.

Received: 14.10.2002